Quench Considerations and Protection Scheme of a High Field HTS Dipole Insert Coil

E. Härö, A. Stenvall, T. Lecrevisse, J. Fleiter, J. M. Rey, M. Sorbi, M. Devaux, C. Trophime, P. Fazilleau, G. Volpini, P. Tixador, F. Hornung, and C. Pes

***Abstract*—The large scale particle accelerators of the future in the 20 T regime are enabled by high temperature superconducting magnets. The dipole magnets needed in new high-field accelerators can be constructed with an YBCO insert and a Nb_3Sn outsert. Such a configuration makes the quench analysis and magnet protection challenging because the quench behavior in both of these coils is different and there is very strong inductive coupling between the coils. The Nb_3Sn coil is characterized by high energy and current and relatively fast quench propagation velocity. However, quench propagates slowly in YBCO coils because of typically wide spread large temperature margin. Currently, in the EuCARD project, a European collaboration is targeting to construct a small-scale high field YBCO-Nb_3Sn hybrid magnet. In this paper, we scrutinize quench in the YBCO insert. We utilized an approach based on a solution of the heat diffusion equation with the finite element method. Additionally, we present a protection scheme for the coil.**

***Index Terms*—High temperature superconductors, quench simulation, stability analysis, superconducting magnets.**

I. Introduction

THE QUENCH dynamics of low temperature superconductors (LTS) are well-known and documented [1, Ch. 9]. In addition, their simulation models have been extensively studied [2], [3]. As opposed to the local hot spot of a LTS magnet it has been proposed that the stability of a high temperature superconductor (HTS) magnet is lost due to global temperature increase in the magnet [4] due to the index loss [5]. However, in a reliable HTS magnet design there is typically a wide margin between current sharing temperature and operating temperature. When this is accompanied with rapidly increasing specific heat as a function of temperature, HTS magnets are extremely stable for operation. However, HTS wires suffer from inhomogenous critical currents [6], especially when manufactured in long lengths, and manufacturing of a magnet can easily lead to local degradation of a wire. Thus, often stability is lost in HTS magnets due to locally decreased critical current [7].

In a European project, views on possible future upgrade of LHC in CERN are being studied. One possible approach, to increase the particle energy, needs upgrade of the dipoles to about 20 T fields [8]. Within this framework a European consortium is formed to design and construct a 19 T superconducting pre-accelerator dipole from a Nb_3Sn outsert and an YBCO insert [9]. This program is coordinated by EuCARD (European Coordination for Accelerator Research and Development) project WP7 Superconducting High Field Magnets for higher luminosity and energies [10].

In this paper we scrutinize quench and protection of the YBCO insert, which is operating in a background field of 13 T produced by Nb_3Sn outsert. However, only YBCO insert quench dynamics are studied in this paper. First, we present the computational model for the quench analysis and then consider proposed magnet protection system. Finally, we present results for temperature increase in the insert due to a quench caused by local degradation of the HTS cable.

II. Computational Model

A. HTS Insert Configuration and Geometry

To produce total magnetic flux density of 19 T, a racetrack type YBCO coil producing 6 T is inserted in a block coil design dipole Nb_3Sn outsert having a bore field of 13 T at 4.2 K with nominal operating current [8]. The Nb_3Sn outsert, called FRESCAII, is an update to FRESCA facility at CERN [12]. FRESCAII has a bore with length of 730 mm and diameter of 100 mm for testing superconducting cables as well as the HTS insert, thus, leading to an outer diameter of the HTS insert of 99 mm to allow its insertion [9], [11], [13]. This magnet has the bore width of 10 mm, but does not allow insertion of a beam pipe since the ends are not bent.

Preliminary tape configuration for the insert is shown in Fig. 1. The conductor is made by assembling two 12 mm wide YBCO tapes together with copper layer in the middle for connection. Then, two of these cables are connected in parallel. This configuration is used to get flexible enough high current HTS cable. In principle, Roeble cable would be currently the best option, but they are not yet mature enough for such magnet development [14].

Taking into account the 99 mm restriction of the external diameter and 12 mm height of the pancake (tape width), the insert design consists of 6 pancakes (Fig. 2 and Table I [9]). Only 1/8th of the geometry is shown in Fig. 2 (Full model of the insert is shown in Fig. 7). The relative proportions of the coil unit cell materials are presented in Table II.

This work was supported by the European Commission under the FP7 Research Infrastructures project EuCARD, Grant 227579, Stability Analysis of Superconducting Hybrid Magnets (Academy of Finland, no. 250652), and Electromagnetic Analysis of Enhanced MgB_2 Superconductors (Academy of Finland, no. 131577). This work is part of EuCARD Work Package 7: Superconducting High Field Magnets for higher luminosities and energies.

E. Härö and A. Stenvall are with Tampere University of Technology, Electromagnetics, FIN-33101 Tampere, Finland (e-mail: erkki.haro@tut.fi).

M. Sorbi and G. Volpini are with INFN Sezione di Milano LASA, Milano 20090, Italy.

J. Fleiter is with CERN, Geneva 23 1211, Switzerland.

P. Fazilleau, T. Lecrevisse, J. M. Rey, M. Devaux, and C. Pes are with the CEA-DSM-IRFU-SACM, Gif sur Yvette 91191, France.

C. Trophime and P. Tixador are with the G2Elab/Institut Néel, Grenoble INP, 38042 Grenoble, France.

F. Hornung is with Karlsruhe Institute of Technology, Institute for Technical Physics, D-76344 Eggenstein-Leopoldshafen, Germany.

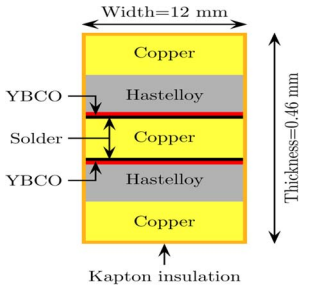

Fig. 1. Tape configuration with insulation layer used in quench computations. Figure is not to scale.

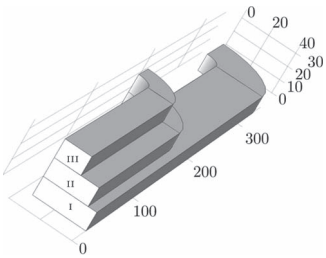

Fig. 2. 1/8th of the insert geometry used in computations. Dimensions are in millimeters.

TABLE I
MAGNET CHARACTERISTICS [9]

Pancake	Number of turns	Length (mm)
I mid plane	73	700
II medium	61	350
III top	35	326.1

TABLE II
RELATIVE MATERIAL PROPORTIONS OF COIL UNIT CELL

Copper	33 %
Hastelloy+YBCO	17 %
Tin Solder	25 %
Epoxy Resin + Kapton	25 %

B. Computational Model for Quench Analysis

Analysing quench dynamics is a challenging task for which multiphysics modeling is required. Our approach to scrutinize quench is to combine the magnetostatics problem with the heat diffusion equation and adequate circuit model due to external protection. The field problems are solved with the finite element method (FEM) in 3D. For future hybrid magnet modeling, it is profitable to create tailored software specifically for quench modeling without restrictions from commercial sources.

Our software is built inside an open-source code, namely GMSH [15]. In principle, GMSH project allows worldwide distribution of the developed software with modern software engineering tools. A Riemannian manifold interface in the GMSH has been selected for the environment to present models and relevant field quantities [16]. The implementation of the Riemannian interface based on axioms in structural mathematics and their models allows flexible multiphysics modeling with the tools of modern mathematics. This means that all the models can be built with the language of differential topology and geometry [17], [18, Ch. 2-3]. This has lately been utilized in our community in case of modeling of ac-losses and critical currents of twisted wires [19], [20].

The block diagram of the quench software is presented in Fig. 3. First we computed magnetic field density in the

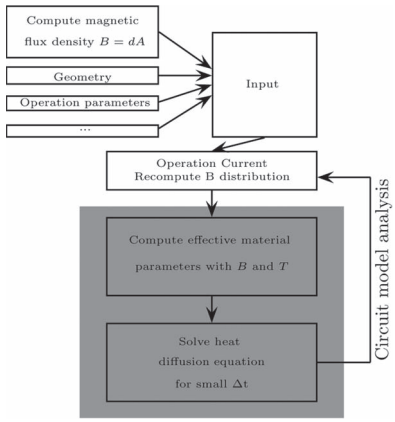

Fig. 3. Block diagram of the computational model.

modeling domain. This was done by solving magnetic vector potential A from the magnetostatic problem

$$\mathrm{d} \star \frac{1}{\mu} \mathrm{d}A = J, \tag{1}$$

where d is the exterior derivative [18, Ch. 14], $\star$ is the Hodge star operator [18, p. 73], μ is the permeability and J the current density. It was possible to exploit the symmetry, thus, the problem was solved only in 1/8th of the insert geometry. Whitney edge elements were employed in the discretization of A [21]–[23].

Detailed representation of the HTS magnet in the level of layered YBCO tapes is not possible due to the complex nature of the tape. Thus, we exploited homogenized material parameters.

The effective volumetric heat capacity C was computed according to [4]. The specific heat values of copper and epoxy resin were interpolated from data given in [24, p. VIII-B1] and that of hastelloy was taken from [25]. For kapton, properties of epoxy resin were used. For the tin solder values of copper were used. YBCO and buffer layers of coated conductor were not considered on the material properties, since their volumetric contribution on the coil is only under 0.5% and, for this study, we assumed their effect to be negligible.

Anisotropic effective thermal conductivities (λ) were used according to the model presented in [4]. Different thermal conductivity values were used for copper [24, p. VII-B2.1], epoxy resin [26], hastelloy [25], and tin solder [27, p. 579]. RRR of copper was 100.

With these material properties we solved the heat diffusion equation

$$\mathrm{d}\lambda \star \mathrm{d}T + Q = C\partial_{\mathrm{t}} T, \tag{2}$$

where T is the temperature and Q the heat generation. Unlike magnetostatic problem, however, the heat diffusion equation has to be solved in the whole coil volume because symmetry cannot typically be exploited. However, in an HTS coil, quench propagates slowly and large part of the geometry does not contribute to the results. The possibility to exploit this knowledge in the modeling will be studied in the future.

Heat generation inside the magnet was computed according to the current sharing model [1, p. 91–92]. For computing the effective resistivity of the matrix metal, we used model from [28]. Different resistivity values for copper [29], hastelloy [25], and tin solder [27, p. 611] were used.

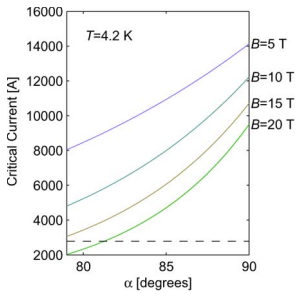

Fig. 4. YBCO cable critical current as a function of field angle. Dashed line represents the nominal operating current of 2800 A.

When the new temperature distribution is solved using (2) the circuit model can be used to update operation current. In Fig. 3, the gray box illustrates the nonlinear part of our software, which solves effective material parameters while solving for (2).

The critical current of the assembled YBCO cable in the parallel direction to the cable was computed from

$$I_c(T,B) = I_0(T)\frac{1}{\left(1+\frac{B}{B_{\mathrm{peak}}(T)}\right)^{\beta}}, \qquad (3)$$

where $I_0(\mathrm{T})$ is the I_c value at 0 T, $B_{\mathrm{peak}}(\mathrm{T})$ is the magnetic flux density corresponding to the maximal macroscopic pinning force and the constant parameter β is 1.43 [30]. Angular dependency of I_c from B was taken into account by formula

$$I_c(B,\theta) = I_c(T,B)\exp\left(\frac{-\|90-\theta\|}{\beta_0 \mathrm{B}^{-\mathrm{d}}}\right), \qquad (4)$$

where θ is the angle of magnetic flux density to the parallel direction of the tape's wide surface and β_0 and d are 62.864 and -0.727, respectively. Critical current computed with (3) and (4) is presented in Fig. 4.

III. Protection Scheme

Protecting the magnet from quench is crucial no matter how well the magnet is stabilized. The simplest way to protect a superconducting magnet is to use external dump resistor [1, pp. 219–221] . Thus, when the quench is detected the power supply will be detached from the circuit and part of the energy of the magnet is dumped in the resistor. However, if the magnet is protected only with a dump resistor, the terminal voltage over the coil might get dangerously high and lead to a breakdown or to a too slow current decay, resulting in too high hot spot temperature.

In order to speed up the current decay after the quench detection, we propose a circuit with gate turn-off thyristors (GTO) to increase step-wise the resistance of the circuit during the current decay. With the proposed circuit, shown in Fig. 5, switch A is opened when the quench is detected and switch B is opened when the current is small enough to put the insert in open circuit. The whole protection circuit is located in room temperature. Using this protection method there are no problems with induced currents, when FRESCAII quenches, due to mutual coupling because the insert can be discharged before the FRESCAII quench protection is activated.

Circuit analysis for current decay and terminal voltage was scrunitized using the proposed protection circuit. Parameters for circuit analysis are presented in Table III.

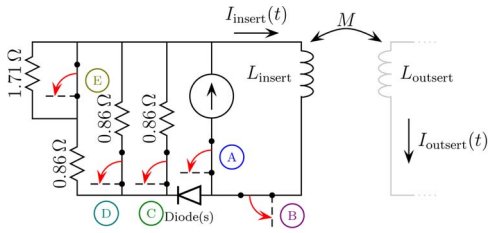

Fig. 5. Proposed protection circuit. A and B denote mechanical circuit breakers and C, D, and E are gate turn-off thyristors.

TABLE III
Parameters for Protection Study

Parameter	Value
Insert Inductance	4 mH
FrescaII inductance	65 mH
Mutual Inductance	9.3 mH
Insert Operation Current	2800 A
Self Energy of Insert	15.68 kJ
FrescaII Operation Current	10500 A
Self Energy of FrescaII	3.4 MJ
Total Energy, including mutual	3.5 MJ
Maximum Insert Terminal Voltage	800-1000 V

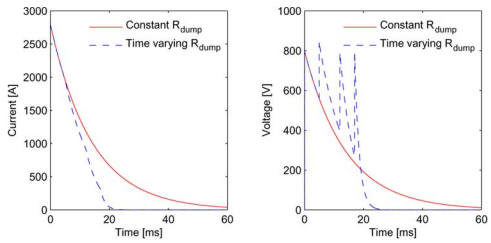

Fig. 6. Circuit analysis results with the proposed protection scheme.

Maximum allowable terminal voltage is around 1000 V, thus, in this analysis we have limited it to even more careful value of 800 V, which leads to a maximum constant dump resistor value of 290 mΩ at operation current. Current decay with presented protection circuit is presented in Fig. 6(a). Current decay can be reduced to about 20 ms compared to a decay time of over 60 ms with a constant resistor, however, the opening time of the mechanical switch is not included. Fig. 6(b) displays the terminal voltage during the current decay which illustrates the change in voltage for faster current decay but without exceeding the voltage criterion of 800 V. The spikes in voltage occurs when the dump resistance value is changed. In the initial state, all the GTOs are closed. At 5 ms, C is opened. Then, at 12 ms D is opened and finally at 17 ms E is opened.

IV. Results from Quench Analysis

Quench was triggered in our computations by introducing in the uppermost pancake a 15 mm long and 0.8 mm wide area with a degraded critical current below the operation current. This way we could get rid of triggering heat pulses, which typically raise the initial temperature of the hotspot unnecessarily high and causes too long normal region. Quench was scrutinized without quench detection or protection to observe the thermal behavior of the system if quench is not detected for some reason. On the other hand, this produces only a slightly pessimistic estimate for hotspot temperature since after the detection and operation of a mechanical switch the current decays in 20 ms with the proposed protection circuit.

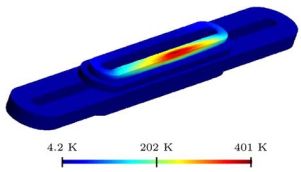

Fig. 7. Temperature distribution from quench computation.

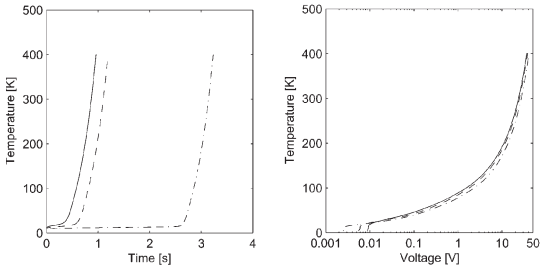

(a) (b)

Fig. 8. Quench simulation results of the YBCO insert. The solid $(-)$ line corresponds to a reduced critical current of 0 A, dashed $(--)$ line 1000 A and dash-dotted $(-.-)$ line 2000 A.

Temperature distribution in the coil area after reaching the value of 400 K is presented in Fig. 7. Like predicted, in an HTS coil the normal zone propagates very slowly. Only half of the uppermost pancake is above 20 K when the hotspot temperature reaches 400 K.

Hotspot temperature as a function of time with different reductions in critical current is presented in Fig. 8(a). It can be seen that after about 0.5 s after the stability is lost the hotspot temperature of 400 K is reached. The critical current degradation has a significant contribution to the time from the start of the simulation until the stability of the magnet is lost. However, the level of the degradation of the critical current does not affect considerably on the rate of temperature rise after the stability is lost.

Hotspot temperature as a function of coil terminal voltage is presented in Fig. 8(b). With the cable used in these computations the terminal voltage is almost 13 V when the temperature of 200 K is reached, thus, quench would have been detected in time, because typical quench detection threshold voltage is 100 mV. After the stability is lost voltage starts to raise very rapidly with temperature which should lead to quench detection. However, this temperature rise is very fast and interference in the measured voltage signal, due to induced voltage when ramping the magnet, can prevent quench detection, thus, leading to magnet breakdown. This can be a severe problem at least when using different type of cable with lower operation current but the same current density.

V. Conclusions

Quench dynamics of a YBCO insert used with a Nb_3Sn outsert for a particle accelerator application was studied using FEM. Our approach was to scrutinize heat diffusion equation in the coil volume. The results show that the normal zone propagates very slowly in the YBCO insert but with a high current cable, quench should be detected in time. Additionally, a relevant protection scheme for YBCO insert was presented. With the proposed model using gate turn-off thyristors to increase step-wise resistance it was possible to reach very fast current decay time without too high terminal voltages.

References

[1] M. N. Wilson, *Superconducting Magnets*. Oxford, U.K.: Clarendon, 1983.

[2] Y. Eyssa, W. Markiewicz, and J. Miller, "Quench, thermal, and magnetic analysis computer code for superconducting solenoids," *IEEE Trans. Appl. Supercond.*, vol. 7, pp. 159–162, 1997.

[3] L. Bottura, "A numerical model for the simulation of quench in the ITER magnets," *J. Comput. Phys.*, vol. 125, pp. 26–41, 1996.

[4] J. Lehtonen, R. Mikkonen, and J. Paasi, "A numerical model for stability considerations in HTS magnets," *Supercond. Sci. Technol.*, vol. 13, pp. 251–258, 2000.

[5] Y. Lvovsky, "Limiting length in cooling design of HTS magnets," *IEEE Trans. Appl. Supercond.*, vol. 11, pp. 1840–1843, 2001.

[6] Y. Wang *et al.*, "Detecting and describing the inhomogeneity of critical current in practical long HTS tapes using contact-free method," *Cryogenics*, vol. 47, pp. 225–231, 2007.

[7] A. Korpela, J. Lehtonen, R. Mikkonen, and R. Perälä, "Temperature dependent current-voltage characteristics of an HTS coil having a poor resistive joint," *Phys. C*, vol. 386, p. 457461, 2003.

[8] L. Bottura, G. de Rijk, L. Rossi, and E. Todesco, "Advanced accelerator magnets for upgrading the LHC," *IEEE Trans. Appl. Supercond.*, vol. 22, p. 4002008, 2012.

[9] M. Devaux *et al.*, "HTS insert magnet design study," *IEEE Trans. Appl. Supercond.*, vol. 22, p. 4203605, 2012.

[10] EuCARD, European Coordination for Accelerator Research and Development. [Online]. Available: http://eucard.web.cern.ch/

[11] P. Ferracin *et al.*, "Development of the EuCARD Nb_3Sn dipole magnet FRESCA2," *IEEE Trans. Appl. Supercond.*, vol. 23, no. 3, p. 4002005, Jun. 2013.

[12] A. P. Verwei *et al.*, "1.9 K test facility for the reception of the superconducting cables for the LHC," *IEEE Trans. Appl. Supercond.*, vol. 9, pp. 153–156, 1999.

[13] J. M. Rey *et al.*, "HTS Dipole Insert Developments," *IEEE Trans. Appl. Supercond.*, vol. 23, no. 3, p. 4601004, Jun. 2013.

[14] J. Schwartz *et al.*, "Status of high temperature superconductor based magnets and the conductors they depend upon," 2011, arXiv:1108.1634v1.

[15] C. Geuzaine and J.-F. Remacle, "Gmsh: A three-dimensional finite element mesh generator with built-in pre- and post-processing facilities," *Int. J. Numer. Meth. Eng.*, vol. 79, pp. 1309–1331, 2009.

[16] M. Pellikka, T. Tarhasaari, S. Suuriniemi, and L. Kettunen, "Programming interface to Riemannian manifold in finite element environment," presented at the ACOMEN, Liége, Belgium, 2011.

[17] W. Boothby, *An Introduction to Differentiable Manifolds and Riemannian Geometry*. New York: Academic, 1975.

[18] T. Frankel, *The Geometry of Physics*. Cambridge Univ. Press, 2012.

[19] A. Stenvall *et al.*, "Manifolds in electromagnetism and superconductor modelling: using their properties to model critical current of twisted conductors in self-field with 2-D model," in *Cryogenics*, 2012, in press.

[20] V. Lahtinen, M. Lyly, A. Stenvall, and T. Tarhasaari, "Comparison of three Eddy current formulations for superconductor hysteresis loss modelling," *Supercond. Sci. Technol.*, vol. 25, p. 115001, 2012.

[21] A. Bossavit, "Whitney forms: A class of finite elements for three-dimensional computations in electromagnetism," *Proc. IEEE*, vol. 135, pp. 493–500, 1988.

[22] D. Baldomir, "Differential forms and electromagnetism in 3-dimensional euclidean space R^3," *Proc. IEEE*, vol. 133, pp. 139–143, 1986.

[23] O. Bíró, K. Preis, and K. Richter, "On the use of the magnetic vector potential in the nodal and edge finite element analysis of 3D magnetostatic problems," *IEEE Trans. Magn.*, vol. 32, pp. 651–654, 1996.

[24] J. Jensen, W. Tuttle, R. Stewart, H. Brechna, and A. Prodell, "Selected cryogenic data notebook," *Brookhaven National Laboratory*, 1981.

[25] J. Lu, E. Choi, and H. Zhou, "Physical properties of hastelloy C-276 at cryogenic temperatures," *J. Appl. Phys.*, vol. 103, p. 064908, 2008.

[26] J. Lehtonen, R. Mikkonen, and J. Paasi, "Effective thermal conductivity in HTS coils," *Cryogenics*, vol. 40, pp. 245–249, 2000.

[27] J. W. Ekin, *Experimental Techniques for Low-Temperature Measurements: Cryostat Design, Material Properties and Superconductor Critical-Current Testing*. Oxorfd, U.K.: Oxford Univ. Press, 2006.

[28] A. Stenvall, A. Korpela, R. Mikkonen, and G. Grasso, "Stability considerations of multifilamentary MgB_2 tape," *Supercond. Sci. Technol.*, vol. 19, pp. 184–189, 2006.

[29] S.-W. Kim, "Material properties for quench simulation (Cu, NbTi and Nb_3Sn)," 2000, Fermilab TD Note 00-041.

[30] T. Lecrevisse, "Quench propagation in YBCO pancake: Experimental and computational results," *IEEE Trans. Appl. Supercond.*, vol. 23, no. 3, p. 4601805, Jun. 2013.